



Pipe-to-pipe friction welding of dissimilar Al-SS joints for cryogenic applications

Hardik Vyas¹ · Kush P. Mehta^{1,2} · Vishvesh Badheka¹ · Bharat Doshi³

Received: 19 June 2019 / Accepted: 10 January 2020 / Published online: 22 January 2020
© The Author(s) 2020

Abstract

In the present investigation, dissimilar materials such as AA6063 and SS304L having pipe dimensions of 60.33 mm outer diameter and 3.9 mm wall thickness were friction-welded with different conditions of process parameters. Nondestructive tests such as radiography test (RT) and liquid penetration test (LPT) were carried out on the welded pipes in order to qualify weld joint. Thermal shock test and helium leak tests were performed on the successful welded samples in order to check its ability to work with cryogenic application. The results revealed that the pipe-to-pipe configuration of dissimilar Al-SS joints was produced successfully by friction welding using continuous drive. There were no defects presented in the joint area as revealed by RT and LPT. Thermal shock test and helium leak tests have also confirmed the soundness of joints. Higher deformation of Al base material results in the huge flash formation of Al that results in the sleeve formation of Al pipe on SS pipe. The helium leak test has confirmed the soundness of joints without any defects after its testing at 1.2 psi pressure. More than 60% of joint efficiency was obtained from Al-SS friction-welded joints.

Keywords Cryogenic dissimilar joints · Friction welding · SS to al joint · Thermal shock test

1 Introduction

Dissimilar metal joints have attained fame in recent years because of its cost- and weight-effective benefits [1-6]. However, it is a challenging task to obtain dissimilar joints due to differences in physical, chemical and mechanical properties of both the base materials. In order to provide unique solutions, dissimilar joints are the requirement of different engineering fields [1-9]. While referring dissimilar joints, the advantages like high functionality and low cost of productivity are obtained for different industrial applications.

Aluminum (Al) and stainless steel (SS) dissimilar joints are very much in demand for the industries such as cryogenics, spacecraft, defense, high pressurized pipelines, chemical and high vacuum systems. In the case of Al-SS dissimilar system, SS has high-temperature strength, toughness, corrosion resistance and very much suitable for use in various structures, whereas Al has lightweight, low melting temperature, superior corrosion resistance and electrical and thermal conductivities. Joining of Al-SS materials leads to the benefits of these combined properties in addition to aforementioned cost and weight advantages [1, 2]. The fusion welding methods are not effective in the case of Al-SS joints as they form amount of brittle intermetallic compounds (IMCs) at the joint area and result in lower tensile strength, which may easily break any time during the service. Therefore, the solid-state welding processes are suggested, wherein joining occurs below the melting point of the base material. Friction welding is one of the solid-state processes that has proved its suitability on the formation of dissimilar joints with the limiting formation of IMCs [10, 11].

Joining of Al-SS friction welding is reported in different literature. Taban et al. [8] described the inertia drive friction welding method in which the base materials such as 12.5 mm round bar of AA6061-T6 and AISI 1018 steel were

Technical Editor: Lincoln Cardoso Brandao.

✉ Kush P. Mehta
kush_2312@yahoo.com

¹ Department of Mechanical Engineering, School of Technology (SOT), Pandit Deendayal Petroleum University (PDPU), Raisan, Gandhinagar, Gujarat, India

² Advanced Manufacturing and Materials group, Department of Mechanical Engineering, School of Engineering, Aalto University, Espoo, Finland

³ Institute for Plasma Research (IPR), Gandhinagar, Gujarat, India

friction-welded with acquired joint strength of 250 MPa. Kimura et al. [9] studied continuous drive friction welding process with a diameter of 16 mm round solid rod work pieces of AA6063 and 304 austenitic stainless steel by keeping Al at the fixed side and SS at the rotated end in the spindle. They investigated forge pressure and forge time during the friction welding process and observed that the joint efficiency was increased with an increase in friction time and forge pressure. Fukumoto et al. [12] observed that increase in friction time improves the tensile strength, but decreases the hardness of the joint. Meshram et al. [10] performed experiments on dissimilar AISI 4340 to Al6061-T6 friction welding having 15 mm solid rod diameter, with an interlayer of sliver material pre-applied by electroplating on AISI 4340 side. The tensile strength and elongation to fracture were improved with an interlayer coated joints compared to without interlayered joints. Additionally, Fe-Al IMCs were experimentally restored by Al-Ag based compounds which in turn resulted in improved ductility of the joint. Sahin et al. [13] studied dissimilar friction welding wherein 10 mm diameter of solid round bar with AISI 304 austenitic stainless steel and commercially pure aluminum materials were considered. Fukumoto et al. [14] used continuous drive friction welding process for solid bar base materials of AA5052 and austenitic SS304 having 19 mm diameter. They investigated the electrical resistivity measurement of Al to SS joint for evaluating soft or hard metal bonding between Al-SS during the friction welding process. They also investigated friction time effects on joint area and concluded that longer friction time generated thick layer of IMCs. Ashfaq et al. [15] studied modification in edge preparation of work pieces subjected to friction welding for 18 mm diameter of solid round bar AISI 304 SS and AA6061. They observed external edge with 15° angle on the SS side with flat edge of the Al side revealed higher joint efficiency as compared to internal taper and the flat edges on the SS side. Yılmaz et al. [16] studied the effect different process parameters such as friction time and rotational speed, friction pressure, upsetting pressure and upsetting time for AISI 304 stainless steel and pure aluminum cylindrical rod of 9.5 mm diameter. They observed that the thickness of IMCs was governed by these parameters.

In the case of friction welding of Al-SS system, majority of previously published articles are on cylindrical rod configurations. To the best of authors' view, there is only one article available for pipe-to-pipe configuration for Al-SS system, wherein continuous drive friction welding process was used for AA6063-T6 and AISI 304 stainless steel materials having 1.5 mm wall thickness, 16 mm outer diameter and 13 mm inner diameter. They obtained 65% of the joint efficiency of the Al base material at maximum when flash was removed at the time of testing. Considering the interesting joint configuration, joint properties improvement and

cryogenic-based specific application, it is worth to perform investigations on Al-SS pipe-to-pipe configuration. The present article investigates joining of dissimilar Al 6063-T6 pipe and SS304L combination for pipe-to-pipe configuration that has a wall thickness-to-outer diameter ratio of 0.064, wherein the diameter of pipe was as high as 60.33 mm. In addition to DT and NDT, the vacuum test and thermal shock test were developed and performed for aforementioned dissimilar friction-welded joints.

2 Materials and methods

SS 304 L and Al 6063-T6 having 60.33 mm pipe outer diameter with 3.9 mm wall thickness were used as workpiece materials. Pipe-to-pipe configuration was attempted for the present investigation as shown in Fig. 1a, which was having a wall thickness-to-outer diameter ratio of 0.064. As the wall thickness-to-outer diameter ratio was below 0.1, the joint configuration was very different and challenging, also reported by Ashfaq et al. [15]. The chemical compositions and mechanical properties of the base metals are given in Tables 1 and 2, respectively.

Welding was performed on a fully automatic continuous drive friction welding machine of 150 T capacity, as shown in Fig. 1b. Four different combinations of process parameters were considered during experimentation, based on past investigations. Table 3 describes the welding parameters for each trial. In all these cases, SS 304 L pipe was fixed in the rotating chuck, while Al 6063-T6 was kept stationary on the other side. Each mating surface of Al-SS joints was properly cleaned with the help of acetone in order to remove dirt impurities from the surfaces.

After performing welding on the mentioned parameters, the welded samples were subjected to testing and characterizations. Initially, the visual inspection was carried out to observe the flash effect. After the visual inspection, the flash was removed from each sample with the help of machining such as turning and boring. The liquid penetration test was performed to check the surface defect in the weld area. Further, the radiography test was performed to check the soundness of the joint. There were three films produced from each welded joint in order to cover the higher diameter of the pipe. The samples were prepared for helium leak test performed on helium leak detection machine. The thermal shock test was carried out by dipping in liquid nitrogen to see the behavior of joint at 77 K. The tensile properties of the welds were assessed according to standard ASME SEC IX, wherein the specimens were sectioned across the welded joint as shown in Fig. 2. These tensile samples were sectioned with the help of wire-cut electric discharge machining.

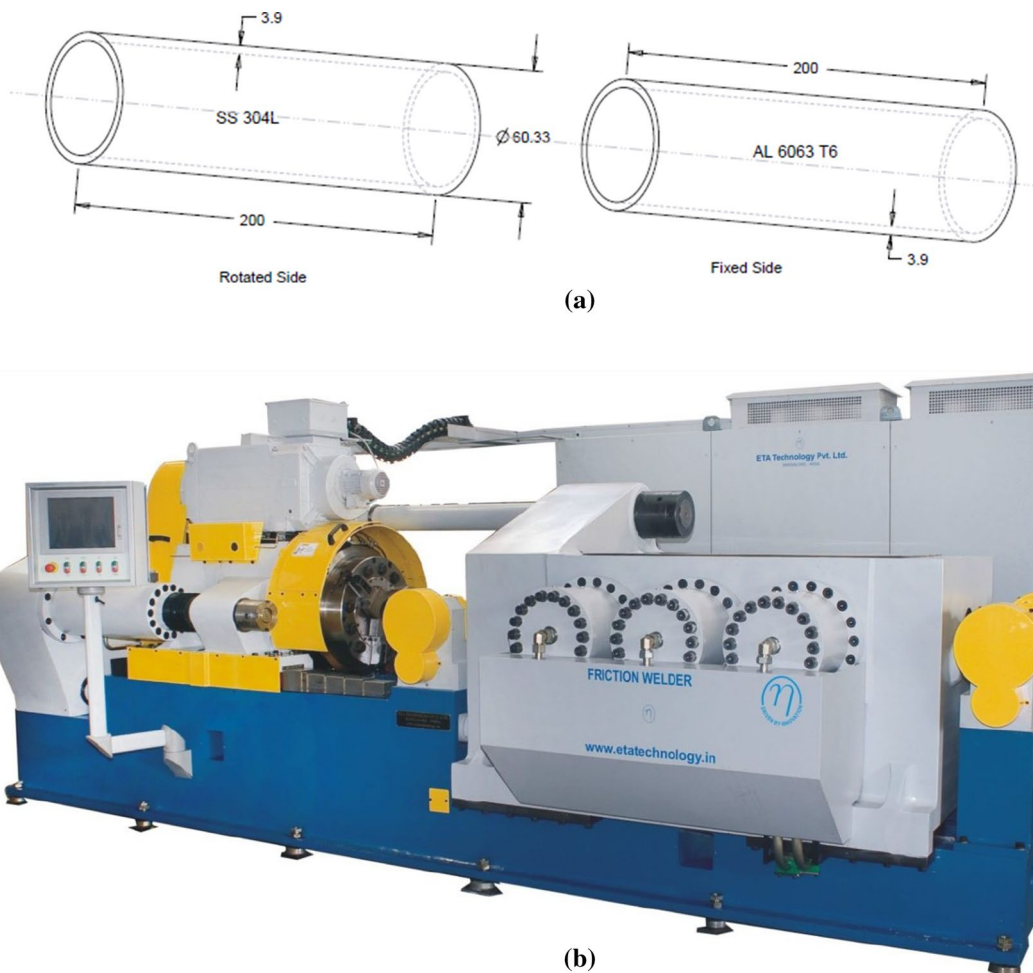


Fig. 1 a Schematic of design in base material pipes (all the dimensions are in mm). b Horizontal friction welding machine

Table 1 Chemical compositions of base metals in wt.%

| SS304L element | C | Mn | Si | Cr | Ni | P | S | Fe |
|--------------------|------|------|------|-------|------|-------|------|---------|
| wt.% | 0.03 | 2.0 | 0.75 | 18.30 | 8.0 | 0.042 | 0.03 | Balance |
| Al 6063-T6 element | Mg | Si | Cu | Fe | Mn | Cr | Zn | Al |
| wt.% | 0.90 | 0.50 | 0.10 | 0.32 | 0.10 | 0.10 | 0.08 | Balance |

Table 2 Mechanical Properties of Base Metals

| | Yield strength (YS) (N/mm ²) | Ultimate tensile strength (UTS) (N/mm ²) | % Elongation |
|------------|--|--|--------------|
| SS304L | 210 | 578 | 76.56 |
| Al 6063-T6 | 208 | 260 | 23.18 |

3 Results and discussion

3.1 Visual inspection

The visual inspection of flash geometry is shown in Fig. 3. Figure 3a shows flash effect on external surface of the pipes, whereas Fig. 3b presents flash effect inside the pipes. All the joints were flashed from the Al side, due to the high amount of deformation of the Al side that was caused because of differences in deformation behavior and flow strength between Al and SS. The authors reported that the length of the Al pipe was decreased to approx.

Table 3 Welding process parameters

| Parameters | Sample Ids | | | |
|-------------------------------------|------------|-------|-------|-------|
| | A | B | C | D |
| Spindle speed (RPM) | 350 | 350 | 350 | 350 |
| Soft force (tones) | 0.5 | 1 | 1 | 0.5 |
| Soft force time (s) | 20 | 20 | 20 | 20 |
| Friction force (tones) | 4.34 | 4.34 | 3 | 3 |
| Friction burn-off displacement (mm) | 6.5 | 6 | 4 | 4 |
| Upset force (tones) | 6 | 6 | 5 | 5 |
| Upset burn off (mm) | 16 | 12 | 6.5 | 13 |
| Burn-off high displacement (mm) | 12 | 12 | 12 | 12 |
| Total burn off (mm) | 22.53 | 17.53 | 11.36 | 17.05 |
| Burn-off low displacement (mm) | 6 | 6 | 6 | 6 |
| Upset time (s) | 5 | 5 | 5 | 5 |

10–12 mm, besides SS pipe length remained the same. It was also observed that large flash formation of sample A was also covering SS materials and seemed like sleeve of Al on SS for 10–12 mm. This was due to quick deformation of Al as compared to SS. Additionally, high-pressure application leads to forming process and subsequently led it to form sleeve of Al (soft material) on SS (hard material) [8]. Moreover, the differences in the flash formation of the Al side can be seen from Fig. 3 relative to each condition. The welded joint of sample A was having a large flash formation, while the welded joint of sample D was flashed less among all. This was due to differences in the process parameters such as friction force and friction

burn-off displacement. In the case of sample A, both of these parameters were higher values relative to other samples and hence resulted in such high flash effect.

3.2 Nondestructive tests

3.2.1 Liquid penetrant test

Liquid penetrant test was performed on all the samples after removing flash from both the sides. The results of liquid penetrant tests are presented in Fig. 4. No major imperfections were observed on the surface of the welds that in turn confirms the soundness of the joints.

3.2.2 Radiography test

The X-ray radiography was performed to confirm the soundness of the weld joints. Radiography test was carried out as per ASTM standards for all the samples. The following conditions were used during radiography testing, as shown in Table 4.

Radiography test results are presented in Table 5. Figure 5 shows the radiography film reports of friction-welded samples. It was observed that the welds were defect-free from the weld zone based on acceptable film results of radiography. This confirms the soundness of the joints, and further these samples were subjected for the rest of the testing and characterizations.

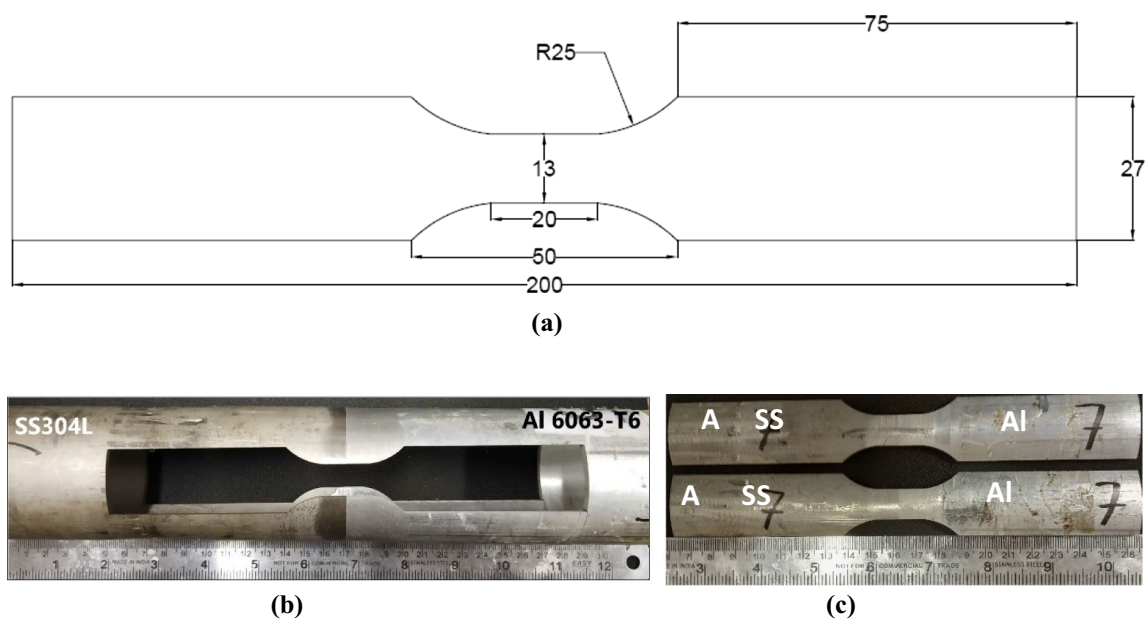


Fig. 2 a Tensile specimen preparation as per ASME Section IX (all the dimensions are in mm). b Welded pipe after extraction of tensile specimens. c Extracted tensile specimens

Fig. 3 Flash shape for different parameters. **a** Outside flash. **b** Inside flash

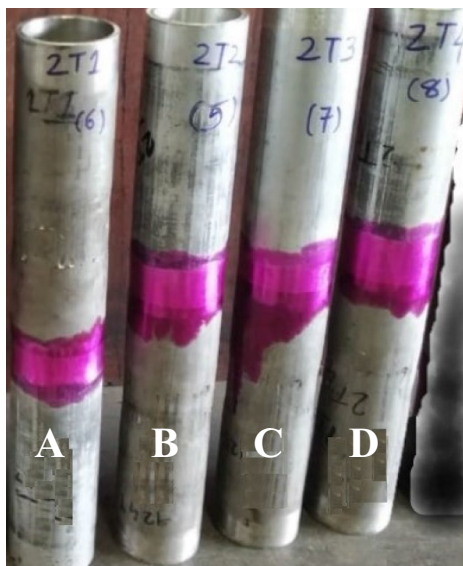
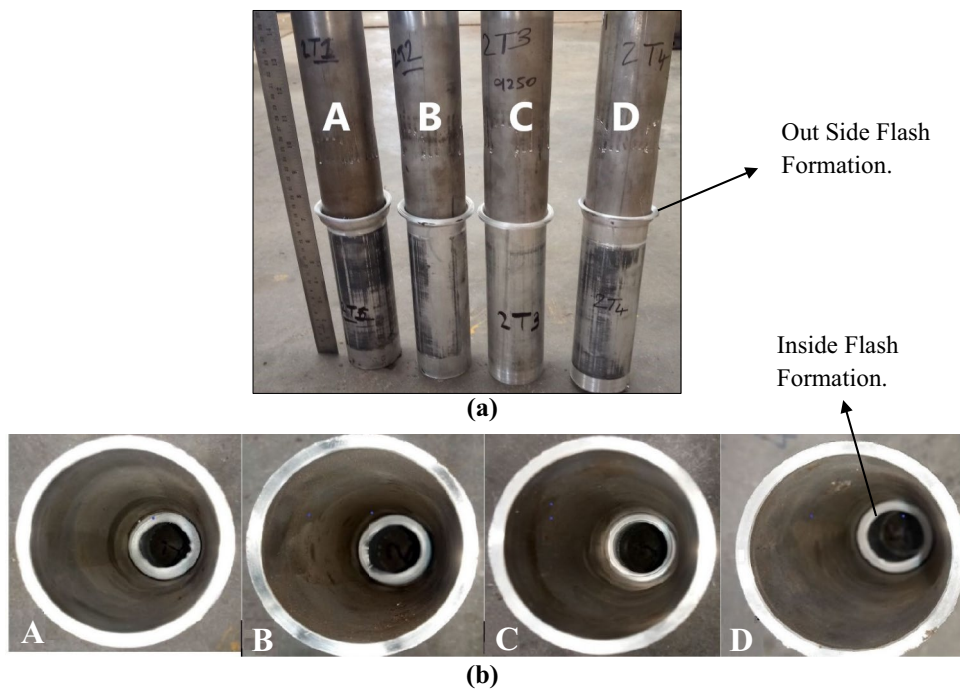


Fig. 4 Liquid penetrant test samples

Table 4 Radiography Testing Conditions

| | | |
|--|----------------------|---------------------|
| Radiation:- X-ray Kv | Exposure: 0.3 mA.min | Processing:- 05 min |
| Screen:- lead | Front:- 0.10 mm | Back:- 0.10 mm |
| Technique—DWSI (double wall, single image) | | |

Table 5 Radiography test results of full pipe diameter

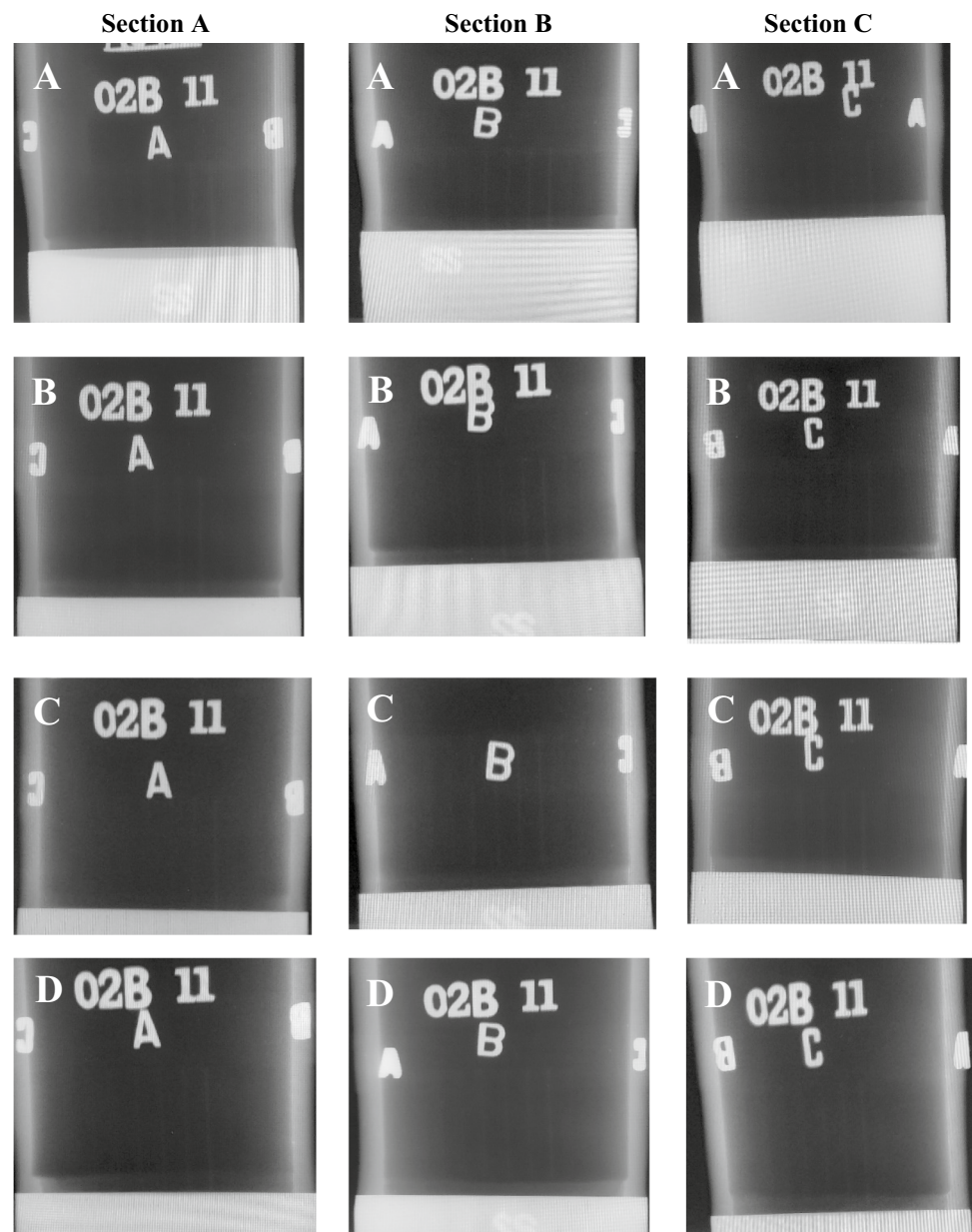
| Sample Ids | Thick-ness (mm) | Full size (inch) | Position | Observation | Remarks |
|------------|-----------------|------------------|----------|-------------|---------|
| A | 3.9 | 4×5 | A | N.S.D | Accept |
| | | | B | | |
| | | | C | | |
| B | 3.9 | 4×5 | A | N.S.D | Accept |
| | | | B | | |
| | | | C | | |
| C | 3.9 | 4×5 | A | N.S.D | Accept |
| | | | B | | |
| | | | C | | |
| D | 3.9 | 4×5 | A | N.S.D | Accept |
| | | | B | | |
| | | | C | | |

N.S.D* No significant defect

3.2.3 Vacuum and thermal shock test

Vacuum test and thermal shock tests were performed to ensure the working of weld in cryogenic temperature and pressurized liquid flow. The preparation of welded joints for vacuum test is shown in Fig. 6, wherein SS reducer and vacuum coupling were attached to SS pipe, while Al flat plate was connected to Al pipe using gas tungsten arc welding. These prepared chambers were mounted on vacuum testing machine as shown in Fig. 7, and the helium was sprayed

Fig. 5 Radiography images



inside the joint area in order to confirm the leak-proof behavior of the joint. Table 6 shows the results of this vacuum test at room temperature. There was no leakage observed during this testing when helium-sprayed at 1.2 psi.

In the case of thermal shock test, the welded samples were dipped in liquid nitrogen at 77 K ($-195.79\text{ }^{\circ}\text{C}$) temperature for 5 min and then pulled out of the liquid and kept aside in the atmosphere in order to allow it to reach the room temperature, i.e. 300 K ($27\text{ }^{\circ}\text{C}$). This was repeated for three times. The reason for doing this exercise was allowing a joint area for free expansion and compression when subjected to cryogenic temperature to room temperature. The differences in compression and expansion ratio of Al and SS base material lead to leakage when subjected to liquid nitrogen

or helium fluid. As both of the pipe materials have different expansion and compression ratios, the joint area must be evaluated for thermal shock test. The results show that the joints have successfully undergone thermal shock test, confirmed through helium leak tests performed after the thermal shock test. The results of a thermal shock test and vacuum test are shown in Fig. 8 and Table 7, respectively.

Figure 9 shows the results of the vacuum leak test before and after the thermal shock test. It can be seen that the vacuum condition was improved drastically after thermal shock test compared to before condition of thermal shock test. The primary reason for this is a low-temperature strengthening effect, which can occur when material experiences a thermal cycle from high temperature to low temperature



Fig. 6 Samples are prepared for vacuum and thermal shock test

[12]. In the case of present investigation, the welds have experienced thermal shock test from room temperature to very low temperature of helium such as 77 K. There were leak proof joints witnessed even after thermal shocks. The vacuum pressure inside the welds was sustained at applied helium spray at 1.2 psi pressure. The strong bonding had

resulted in leak proof joints. The leak proof joints after thermal shock test have resulted in better vacuum conditions compared to room temperature because of aforementioned low, strengthening effects and possible grain refining effects due to plastic strain [17] on the Al side due to thermal shock test from room temperature to cryogenic temperature. Cai et al. [18] noted that vacuum test results were improved with improvements in strength and micro-hardness due to grain refinement caused by the cryogenic treatment.

3.3 Destructive test

3.3.1 Tensile test

Table 8 and Fig. 10 show tensile testing results of dissimilar Al–SS welds. The ultimate tensile strength was reported more than 60% of the Al base material, which confirms the soundness of the joint for the dissimilar materials. Similar results were obtained by Kimura et al. [11] in the case of thin-walled pipe-to-pipe configuration. The yield strength and % elongation were reported low as compared to base materials. Formation of the IMCs may be the reason for this low values of specimens fractured from the Al–SS welded interface. This is may be due to the presence of large and thick IMCs layer at the interface. The formation of IMCs at the interface was reported in

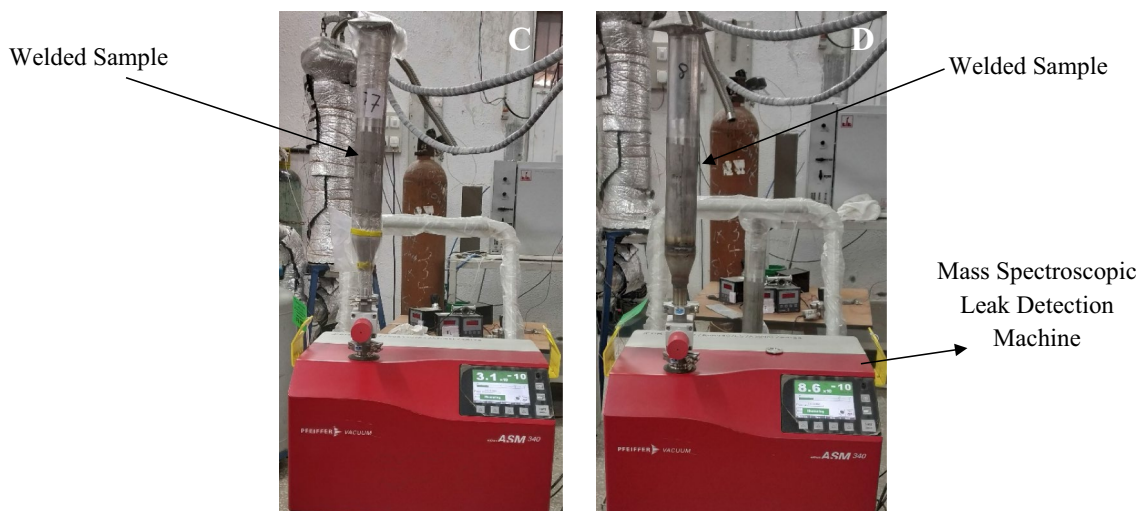


Fig. 7 Vacuum test with mass spectroscopic leak detection machine and welded samples

Table 6 Vacuum test reading at room temperature

| Sample Ids | A | B | C | D |
|--|---------------------|-----------------------|-----------------------|-----------------------|
| Background reading in m bar l/s | 4×10^{-10} | 4×10^{-10} | 6.5×10^{-10} | 8.5×10^{-10} |
| Helium spray time reading in m bar l/s | 4×10^{-10} | 6.7×10^{-10} | 6.4×10^{-10} | 8.0×10^{-10} |
| Helium spray pressure in psi | 1.2 | 1.2 | 1.2 | 1.2 |
| Results | Pass | Pass | Pass | Pass |

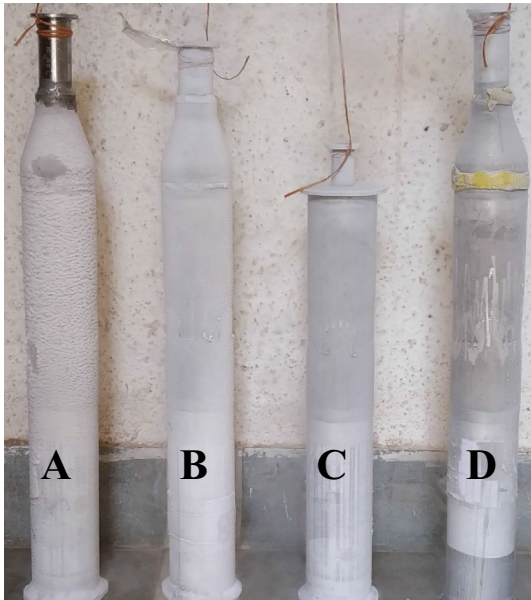


Fig. 8 Thermal shock test at liquid nitrogen temperature (77 K)

many studies [7-16]. The maximum elongation of 15.18% for sample D was reported wherein the fracture location was also observed from the Al base material, as shown in Fig. 11. It was also observed that no major variations in tensile strength were noted that was because of similar heat input conditions that were caused by rotational speed and friction time as largely as compared with the rest of the parameters. These two parameters were not having

major variations and hence may have resulted in similar heat input conditions.

3.3.2 Macrograph and microstructure

Figure 12 shows macro-photograph and micro-photographs of dissimilar friction weld between Al6063-T6 and SS304L for pipe-to-pipe configuration for sample B. From the macrograph (Fig. 12a), it can be seen that there were no major variations observed in the SS side in terms of deformation, while massive deformation can be observed on the Al side. This was due to the differences in the deformation behavior of Al and SS that in turn resulted in interface line between Al and SS. On the Al side near to the interface, different zones were observed such as plastic deformation zone, fully recrystallized zone, partially recrystallized zone and solid solution zone as can be seen from Fig. 12b–g. Besides, no major grain deformation or refinement was observed on the SS side (Fig. 12b). Figure 12d shows that the Al material stretches in the direction of forging movement. This in turn resulted in a deformed zone with elongated grains. The plastic deformation zone was found near to interface et al. side as shown in Fig. 12e. It can be also seen from Fig. 12e that equally distributed recrystallized zone was found on the top side of the pipe. Recrystallization was occurred after sever plastic deformation that was caused due to frictional heat and large forging force. Partial secondary recrystallization was observed toward base material as shown in Fig. 12g, where the combined effects of sever deformation and high temperature were experienced. Figure 12f shows

Table 7 Vacuum test reading after thermal shock test at room temperature

| Sample Ids | A | B | C | D |
|--|-----------------------|-----------------------|-----------------------|-----------------------|
| Background reading in m bar l/s | 1.5×10^{-10} | 2.2×10^{-10} | 1.7×10^{-10} | 1.6×10^{-10} |
| Helium spray time reading in m bar l/s | 1.7×10^{-10} | 2.5×10^{-10} | 1.8×10^{-10} | 1.6×10^{-10} |
| Helium spray pressure in psi | 1.2 | 1.2 | 1.2 | 1.2 |
| Results | Pass | Pass | Pass | Pass |

Fig. 9 Comparison between before and after thermal shock test at room temperature

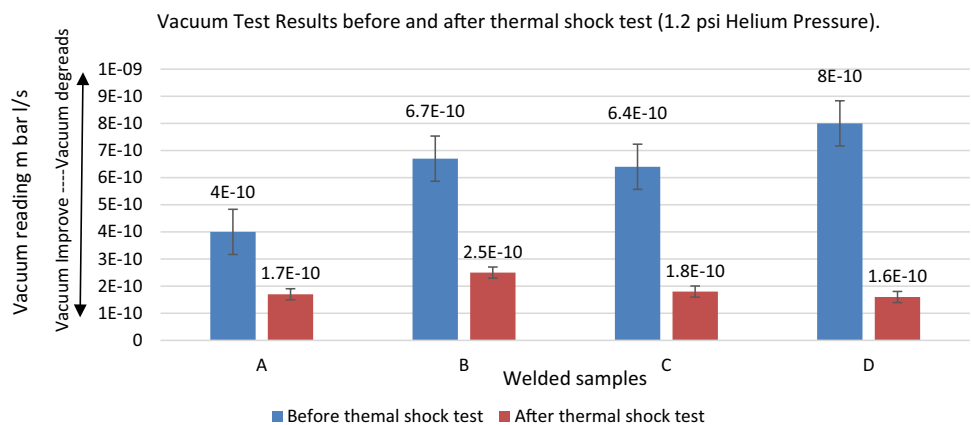
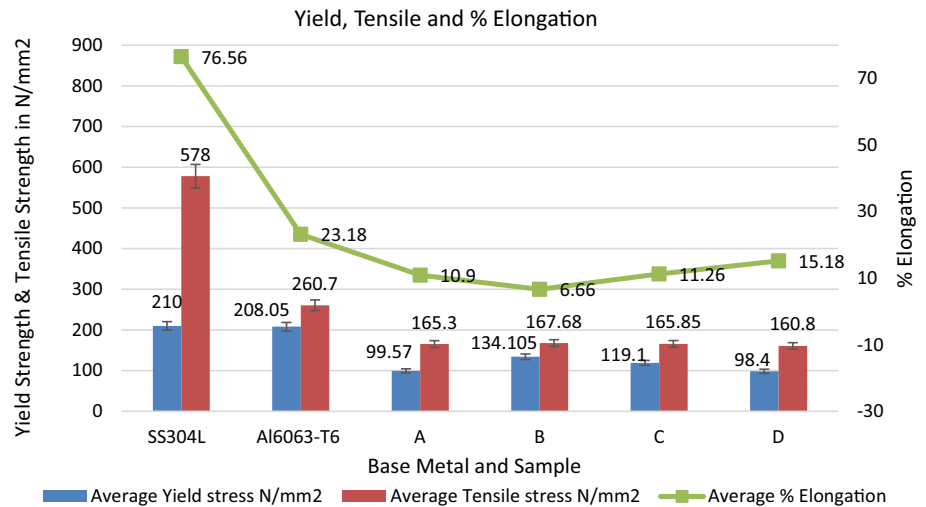


Table 8 Tensile testing results

| Sample Ids | Average yield stress N/mm ² | Average tensile strength N/mm ² | Average % elongation | Remarks on fracture | Joint efficiency % as compared to Al 6063 |
|------------|--|--|----------------------|---|---|
| SS304L | 210 | 578 | 76.56 | Fractured with necking | 100 |
| Al6063-T6 | 208.05 | 260.7 | 23.18 | Fractured with necking | 100 |
| A | 99.57 | 165.3 | 10.9 | Failed from joint area | 61.16 |
| B | 134.105 | 167.68 | 6.66 | Failed from joint area | 66.55 |
| C | 119.1 | 165.85 | 11.26 | Failed from joint area | 65.93 |
| D | 98.4 | 160.8 | 15.18 | Failed from joint area Failed from Al side | 64.46 |

Fig. 10 Effect of parameters on yield strength, tensile strength and % elongation

solid solution zone near the interface area. This region was developed because of adequate precipitation produce by fast cooling rate and higher temperature experiences. The reasons for the formation of different microstructures can be summarized as uneven friction heat distribution and differences in deformation behavior of Al and SS materials [1].

4 Conclusions

- Dissimilar friction welding of Al6063 and SS304L for pipe-to-pipe configuration having an outer diameter of 60.33 mm and a wall thickness of 3.9 mm was successfully obtained.
- Higher deformation of Al base material results in the huge flash formation of Al in the case of Al–SS friction welding. Higher level of frictional deformation results

in sleeve formation of Al on SS base material of pipe-to-pipe configuration.

- There were no defects presented in the joint area as revealed by radiography test and liquid penetrant test.
- The welded joints have successfully experienced vacuum test at room temperature and cryogenic temperature after the thermal shock test. The helium leak test confirmed the soundness of joints without any defects after its testing at 1.2 psi pressure. After thermal shock test, the vacuum results of welded joints were improved because of the low-temperature strengthening effect.
- More than 60% of joint efficiency was obtained from Al–SS friction-welded samples.
- Microstructural variations on the Al side with a distinct interface of Al–SS having different zones such as plastic deformation zone, fully recrystallized zone, partially recrystallized zone and solid solution zone were observed.

Fig. 11 Fracture location of tensile tested specimens

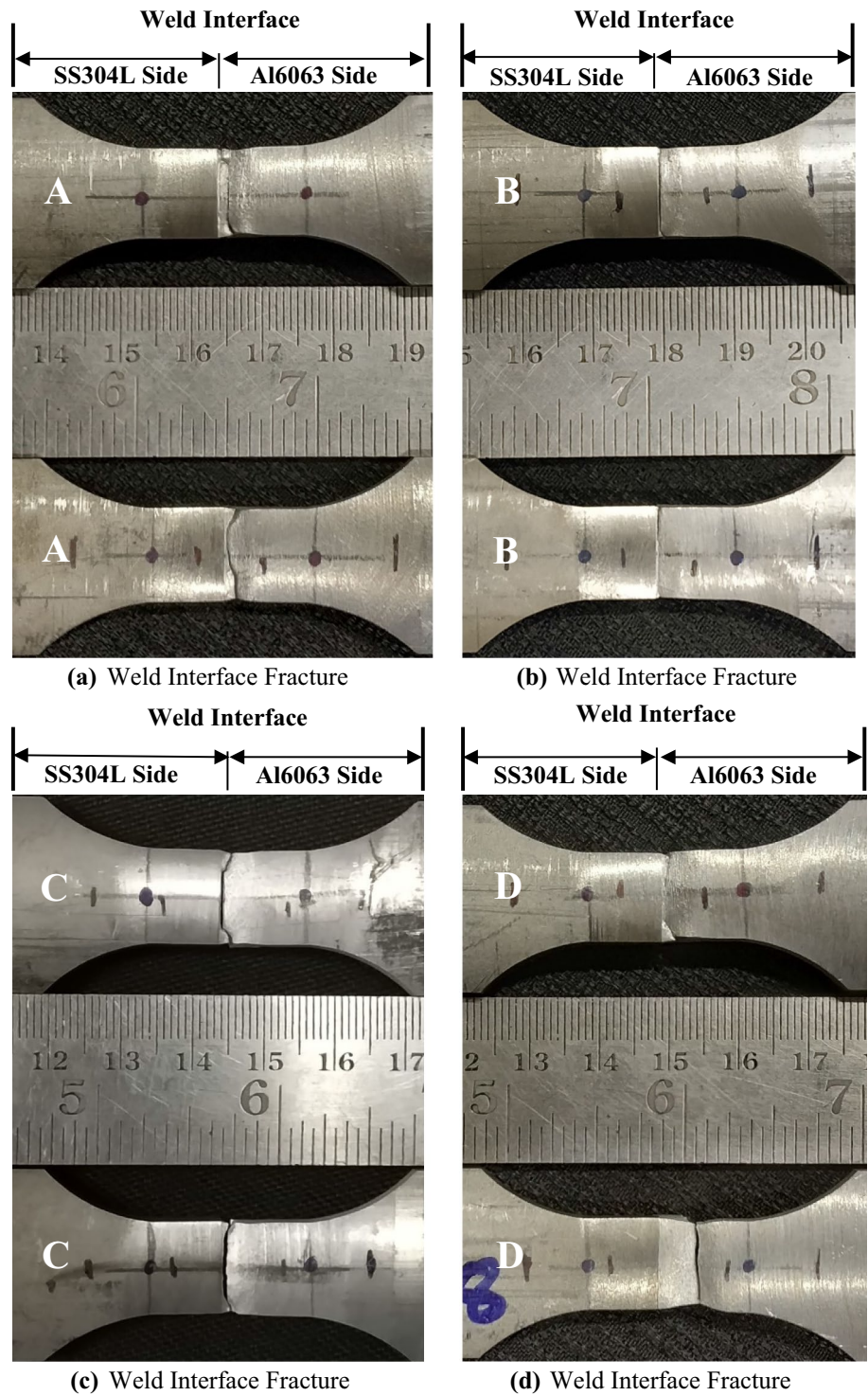
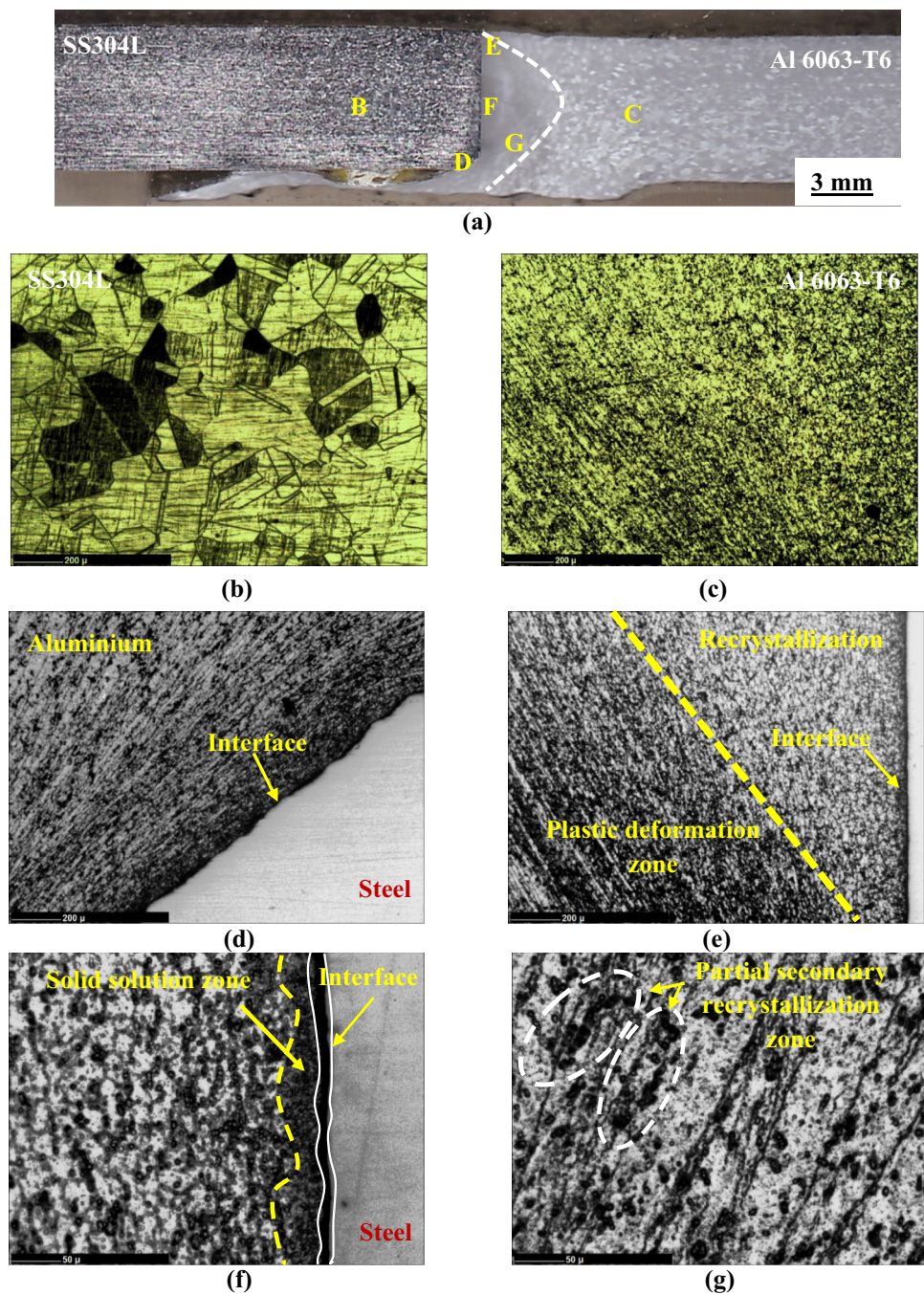


Fig. 12 Optical macrograph and microstructure features of dissimilar Al–SS friction-welded joint of sample B **a** macro-photograph, **b** steel base material microstructure—region B of **a**, **c** aluminum base material microstructure—region C of **a**, **d** Al–steel interface area—region D of **a**, **e** different zones at Al side—region E of **a**, **f** solid solution zone at interface area—region F of **a**, **g** partial secondary recrystallized zone at Al—region G of **a**



Acknowledgements Open access funding provided by Aalto University. The authors wish to express their sincere thanks to Board of Research in Nuclear Sciences (BRNS, Project No: 39/14/02/2018-BRNS/39002), India, for providing the funding. The authors would like to thank M/s Vulcan Industrial Eng. Co. Ltd for providing friction welding machine facility. The authors would also like to express their thanks to Mr. A K Sahu, Scientific Officer-G, Institute for Plasma Research, for providing helium leak and vacuum testing facilities.

Open Access This article is licensed under a Creative Commons Attribution 4.0 International License, which permits use, sharing, adaptation, distribution and reproduction in any medium or format, as long

as you give appropriate credit to the original author(s) and the source, provide a link to the Creative Commons licence, and indicate if changes were made. The images or other third party material in this article are included in the article's Creative Commons licence, unless indicated otherwise in a credit line to the material. If material is not included in the article's Creative Commons licence and your intended use is not permitted by statutory regulation or exceeds the permitted use, you will need to obtain permission directly from the copyright holder. To view a copy of this licence, visit <http://creativecommons.org/licenses/by/4.0/>.

References

1. Mehta K (2017) *Advanced joining and welding techniques: an overview: advanced manufacturing technologies*. Springer, Cham, pp 101–136. https://doi.org/10.1007/978-3-319-56099-1_5.
2. Mehta KP, Badheka VJ (2016) A review on dissimilar friction stir welding of copper to aluminum: process, properties, and variants. *Mater Manuf Processes* 31(3):233–254
3. Mehta KP, Badheka VJ (2016) Effects of tilt angle on the properties of dissimilar friction stir welding copper to aluminum. *Mater Manuf Process* 31(3):255–263
4. Mehta KP, Badheka VJ (2015) Influence of tool design and process parameters on dissimilar friction stir welding of copper to AA6061-T651 joints. *Int J Adv Manuf Technol* 80(9–12):2073–2082
5. Mehta KP, Badheka VJ (2017) Hybrid approaches of assisted heating and cooling for friction stir welding of copper to aluminum joints. *J Mater Process Technol* 239:336–345
6. Mehta KP, Badheka VJ (2017) Influence of tool pin design on properties of dissimilar copper to aluminum friction stir welding. *Trans Nonferrous Metals Soc China* 27(1):36–54
7. Mehta KP (2019) A review on friction-based joining of dissimilar aluminum–steel joints. *J Mater Res* 34(1):78–96
8. Taban E, Gould JE, Lippold JC (2010) Dissimilar friction welding of 6061–T6 aluminum and AISI 1018 steel: Properties and microstructural characterization. *Mater Design* 31(5):2305–2311
9. Kimura M, Suzuki K, Kusaka M, Kaizu K (2017) Effect of friction welding condition on joining phenomena and mechanical properties of friction welded joint between 6063 aluminium alloy and AISI 304 stainless steel. *J Manuf Process* 26:178–187
10. Meshram SD, Reddy GM (2015) Friction welding of AA6061 to AISI 4340 using silver interlayer. *Def Technol* 11(3):292–298
11. Kimura M, Kusaka M, Kaizu K, Nakata K, Nagatsuka K (2016) Friction welding technique and joint properties of thin-walled pipe friction-welded joint between type 6063 aluminum alloy and AISI 304 austenitic stainless steel. *Int J Adv Manuf Technol* 82(1–4):489–499
12. Fukumoto S, Inuki T, Tsubakino H, Okita K, Aritoshi M, Tomita T (1997) Evaluation of friction weld interface of aluminium to austenitic stainless steel joint. *Mater Sci Technol* 13(8):679–686
13. Sahin M (2009) Joining of stainless-steel and aluminium materials by friction welding. *Int J Adv Manuf Technol* 41(5–6):487–497
14. Fukumoto S, Tsubakino H, Okita K, Aritoshi M, Tomita T (1999) Friction welding process of 5052 aluminium alloy to 304 stainless steel. *Mater Sci Technol* 15(9):1080–1086
15. Ashfaq M, Sajja N, Rafi HK, Rao KP (2013) Improving strength of stainless steel/aluminum alloy friction welds by modifying faying surface design. *J Mater Eng Perform* 22(2):376–383
16. Yılmaz M, Çöl M, Acet M (2002) Interface properties of aluminum/steel friction-welded components. *Mater Charact* 49(5):421–429
17. Ding H, Wu Y, Lu Q, Xu P, Zheng J, Wei L (2018) Tensile properties and impact toughness of S30408 stainless steel and its welded joints at cryogenic temperatures. *Cryogenics* 92:50–59
18. Cai Y, Luo Z, Zeng Y (2017) Influence of deep cryogenics treatment on the microstructure and properties of AISI304 austenitic stainless steel A-TIG weld. *Sci Technol Weld Join* 22:236–243

Publisher's Note Springer Nature remains neutral with regard to jurisdictional claims in published maps and institutional affiliations.